

Tessellating the moduli space of strictly convex projective structures on the once-punctured torus

Robert C. Haraway, III and Stephan Tillmann

Abstract We show that associating the Euclidean cell decomposition due to Cooper and Long to each point of the moduli space of framed strictly convex real projective structures of finite volume on the once-punctured torus gives this moduli space a natural cell decomposition. The proof makes use of coordinates due to Fock and Goncharov, the action of the mapping class group as well as algorithmic real algebraic geometry. We also show that the decorated moduli space of framed strictly convex real projective structures of finite volume on the thrice-punctured sphere has a natural cell decomposition.

AMS Classification 57M50, 57N05, 14H15

Keywords Projective surface, cell decomposition, moduli space, convex hull

1 Introduction

Classical Teichmüller space can be viewed as the moduli space of marked hyperbolic structures of finite volume on a surface. In the case of a punctured surface, many geometrically meaningful *ideal cell decompositions* for its Teichmüller space are known. For instance, quadratic differentials are used for the construction attributed to Harer, Mumford and Thurston [15]; hyperbolic geometry and geodesic laminations are used by Bowditch and Epstein [2]; and Penner [21] uses Euclidean cell decompositions associated to the points in *decorated* Teichmüller space. The decoration arises from associating a positive real number to each cusp of the surface. All of these decompositions are natural in the sense that they are invariant under the action of the mapping class group (and hence descend to a cell decomposition of the moduli space of unmarked structures) and that they do not involve any arbitrary choices.

A hyperbolic structure is an example of a *strictly convex projective structure*, and two hyperbolic structures are equivalent as hyperbolic structures if and only if they are equivalent as projective structures. Let $S_{g,n}$ denote the surface of genus g with n punctures. We will always assume that $2g + n > 2$, so that the surface has negative Euler characteristic. Whereas the classical Teichmüller space $\mathcal{T}(S_{g,n})$ is homeomorphic with $\mathbb{R}^{6g-6+2n}$, Marquis [19] has shown that the analogous moduli space $\mathcal{T}_+(S_{g,n})$ of marked strictly convex projective structures of finite volume on $S_{g,n}$ is homeomorphic with $\mathbb{R}^{16g-16+6n}$.

Recently, Cooper and Long [3] generalised the key construction of Epstein and Penner [10], which was used in Penner's decomposition of decorated Teichmüller space [21]. Cooper and Long [3] state that their construction can be used to define a decomposition of the decorated moduli space $\tilde{\mathcal{T}}_+(S_{g,n})$, but that it is not known whether all components of this decomposition are cells.

As in the classical setting, there is a principal \mathbb{R}_+^n foliated fibration $\tilde{\mathcal{T}}_+(S_{g,n}) \rightarrow \mathcal{T}_+(S_{g,n})$, and different points in a fibre above a point of $\mathcal{T}_+(S_{g,n})$ may lie in different components of the decomposition of $\tilde{\mathcal{T}}_+(S_{g,n})$. However, if there is only one cusp, then all points in a fibre lie in the same component, and one obtains a decomposition of $\mathcal{T}_+(S_{g,1})$.

The proofs of cellularity in [10, 21] make essential use of the hyperbolic metric and in particular the Minkowski model for hyperbolic space. One obstacle in finding analogous proofs that work in the setting of projective geometry lies in the fact that the model geometry varies. Whereas every hyperbolic surface is a quotient of the interior of the unit disc, one can only guarantee that a strictly convex projective surface is the quotient of some open strictly convex domain in projective space. But as one varies the projective structure, the domain may change to a projectively inequivalent domain. Moreover, the geometry arises from the Hilbert metric on the domain, which in general is a non-Riemannian Finsler metric.

The main contribution of this paper is to give the first evidence towards a positive answer to the question of whether Penner's result generalises to $\tilde{\mathcal{T}}_+(S_{g,n})$. We also introduce the concept of *trigonal matrices* in §4, which allow computation of holonomy without the introduction of cube roots, and the concept of *cloverleaf position* in §9, which normalises domains to vary compactly.

We show that for the once-punctured torus $S_{1,1}$, the decomposition of $\mathcal{T}_+(S_{1,1})$ is indeed an ideal cell decomposition, which is invariant under the action of the mapping class group. Moreover, there is a natural bijection between the cells and the ideal cell decompositions of $S_{1,1}$. This is stated formally as Theorem 1 in §3. The analogous statement for the decorated moduli space $\tilde{\mathcal{T}}_+(S_{0,3})$ of the thrice-punctured sphere $S_{0,3}$ is also shown (see Theorem 7 in §8).

In addition to giving evidence towards a generalisation of Penner's result, our methods show that on the one hand, the parametrisation due to Fock and Goncharov [12, 13] makes the computation of the decomposition of moduli space feasible, and that it may also provide the right theoretical framework for a general proof. We also show that our computational tools allow a systematic study of deformations and degenerations of strictly convex projective structures in §9 and discuss further directions in §10.

2 Ideal cell decompositions of surfaces

An *ideal cell decomposition* of $S_{g,n}$ consists of a union Δ of pairwise disjoint arcs connecting (not necessarily distinct) punctures with the properties that no two arcs are homotopic (keeping their endpoints at the punctures) and that each component of $S_{g,n} \setminus \Delta$ is an open disc. The arcs are called *ideal edges*. We regard two ideal cell decompositions as the same if they are isotopic (keeping the endpoints of all arcs at the punctures). The set of (isotopy classes of) ideal cell decompositions of $S_{g,n}$ has the structure of a partially ordered set, with the partial order given by inclusion. Given ideal cell decompositions Δ_1 and Δ_2 we always understand statements such as “ $\Delta_1 = \Delta_2$,” “ $\Delta_1 \subseteq \Delta_2$ ” or “ $\Delta_1 \cap \Delta_2 \neq \emptyset$ ” up to isotopy.

For instance, in the case of $S_{1,1}$, an ideal cell decomposition either has two ideal edges and its complement is an *ideal quadrilateral* or it has three ideal edges and its complement consists of two *ideal triangles*. We call the latter an *ideal triangulation* and the former an *ideal quadrilateral* of $S_{1,1}$. An ideal quadrilateral can be divided into two triangles in two different ways, depending on which diagonal is used to subdivide it. The space of all ideal cell decompositions of $S_{1,1}$

is naturally identified with the infinite trivalent tree. Vertices of the tree correspond to ideal triangulations and there is an edge between two such triangulations Δ_0 and Δ_1 if and only if Δ_0 is obtained from Δ_1 by deleting an ideal edge e (hence creating an ideal quadrilateral) and then inserting the other diagonal of the quadrilateral. This is called an *edge flip* or *elementary move*. The ideal cell decomposition $\Delta_1 \setminus \{e\}$ is associated with the edge in the tree with endpoints Δ_0 and Δ_1 .

Floyd and Hatcher [11] identify this tree with the dual tree to the *modular tessellation* or *Farey tessellation* of the hyperbolic plane. An excellent illustration of this (including the information about edge flips) can be found in Lackenby [18]. The tiles in the modular tessellation are ideal triangles with the properties

- (1) each vertex is a rational number or $\infty = \frac{1}{0}$,
- (2) if $\frac{p}{q}$ and $\frac{r}{s}$ are two vertices of the same ideal triangle, then $ps - rq = \pm 1$,
- (3) the set of vertices of each ideal triangle is of the form $\{\frac{p}{q}, \frac{r}{s}, \frac{p+r}{q+s}\}$

The full tessellation can thereby be generated from the ideal triangle with vertices $\frac{0}{1}, \frac{1}{0}, \frac{1}{1}$ and the ideal triangle with vertices $\frac{1}{0}, \frac{-1}{1}, \frac{0}{1}$. Moreover, the element of the mapping class group taking one ideal triangulation to another can be determined from this information.

3 Convex hull constructions

We summarise some key definitions and results that can be found in [19, 8]. A *strictly convex projective surface* is $S = \Omega/\Gamma$, where Ω is an open strictly convex domain in the real projective plane with the property that the closure of Ω is contained in an affine patch, and Γ is a torsion-free discrete group of projective transformations leaving Ω invariant. Since there is an analytic isomorphism $\mathrm{PGL}(3, \mathbb{R}) \cong \mathrm{SL}(3, \mathbb{R})$, we may assume $\Gamma < \mathrm{SL}(3, \mathbb{R})$.

The Hilbert metric on Ω can be used to define a notion of volume on S , and we are interested in the case where S is non-compact but of finite volume. Then the ends of S are cusps, and the holonomy of each cusp is conjugate to the *standard parabolic*

$$\begin{pmatrix} 1 & 1 & 0 \\ 0 & 1 & 1 \\ 0 & 0 & 1 \end{pmatrix},$$

and its unique fixed point on $\partial\Omega$ is called a *parabolic fixed point*.

Cooper and Long [3] associate ideal cell decompositions to cusped strictly convex projective surfaces of finite volume as follows. Suppose $S = \Omega/\Gamma$ is homeomorphic with $S_{g,n}$. The $(\mathrm{SL}(3, \mathbb{R}), \mathbb{R}P^2)$ -structure of S lifts to a $(\mathrm{SL}(3, \mathbb{R}), \mathbb{S}^2)$ -structure. We denote a lift of Ω to $\mathbb{S}^2 \subset \mathbb{R}^3$ by Ω^+ . A *light-cone representative* of $p \in \partial\Omega$ is a lift $v_p \in \mathcal{L} = \mathcal{L}^+ = \mathbb{R}^+ \cdot \partial\Omega^+$. Each cusp c of S corresponds to an orbit of parabolic fixed points on $\partial\Omega$. Choose an orbit representative $p_c \in \partial\Omega$, and hence a light-cone representative $v_c = v_{p_c} \in \mathcal{L}$. The set $B = \{\Gamma \cdot v_c \mid c \text{ is a cusp of } S\}$ is discrete. Let C be the convex hull of B . Then the projection of the faces of ∂C onto Ω is a Γ -invariant ideal cell decomposition of Ω , and hence descends to an ideal cell decomposition of Ω/Γ , called an *Epstein-Penner decomposition* by Cooper and Long.

Varying the light-cone representatives v_c gives a $(n - 1)$ -parameter family of Γ -invariant ideal cell decompositions of Ω . Note that if each face of C is a triangle, then a small perturbation of the lengths of the p_c will not change the combinatorics of C . Also, in the case of one cusp, varying the length of p_c merely dilates C and hence does not change the combinatorics of the convex hull. In particular, the decomposition of the surface Ω/Γ is canonical if $n = 1$. However, if there is more than one cusp, then varying the length of just one p_c will eventually result in different decompositions, since it changes the relative heights of the vertices of C .

To summarise, given $p \in \tilde{\mathcal{T}}_+(S_{g,n})$, the convex hull construction by Cooper and Long [3] associates to p a canonical ideal cell decomposition Δ_p . Analogous to Penner [21], define for any ideal cell decomposition $\Delta \subset S_{g,n}$ the sets

$$\begin{aligned}\mathring{\mathcal{C}}(\Delta) &= \{p \in \tilde{\mathcal{T}}_+(S_{g,n}) \mid \Delta_p = \Delta\}, \\ \mathcal{C}(\Delta) &= \{p \in \tilde{\mathcal{T}}_+(S_{g,n}) \mid \Delta_p \subseteq \Delta\}.\end{aligned}$$

As in the classical case, we have $\mathcal{C}(\Delta_1) \cap \mathcal{C}(\Delta_2) \neq \emptyset$ if and only if $\Delta_1 \cap \Delta_2$ is an ideal cell decomposition of $S_{g,n}$, and in this case $\mathcal{C}(\Delta_1) \cap \mathcal{C}(\Delta_2) = \mathcal{C}(\Delta_1 \cap \Delta_2)$. Moreover, if there is just one puncture, we may replace $\tilde{\mathcal{T}}_+(S_{g,1})$ with $\mathcal{T}_+(S_{g,1})$ in the above definitions.

We can now state the main theorem of this paper:

Theorem 1 *The set*

$$\{\mathring{\mathcal{C}}(\Delta) \mid \Delta \text{ is an ideal cell decomposition of } S_{1,1}\}$$

is an ideal cell decomposition of $\mathcal{T}_+(S_{1,1})$ that is invariant under the action of the mapping class group. Moreover, $\mathring{\mathcal{C}}$ is a natural bijection between the cells and the ideal cell decompositions of $S_{1,1}$.

The proof will be given in §7, and the analogous statement for the thrice-punctured sphere is proved in §8. First, some general results are developed in §4, the computation of holonomy is discussed in §5, and the coordinates for $\mathcal{T}_+(S_{1,1})$ are derived in §6. Possible applications and further directions are discussed in §9 and §10.

4 Projectivity

Fock and Goncharov discovered in [12] that the moduli space of mutually inscribed and circumscribed triangles (from the perspective of some affine patch in $\mathbb{R}P^2$) is naturally isomorphic to the positive real line. We now develop an explicit formulation of this isomorphism, introducing the new concept of a *(standard) trigonal matrix*.

An element of \mathcal{P}_3^+ is the projectivity class of a combination of three points in $\mathbb{R}P^2$ in general position and three lines through those points such that, from the perspective of some affine patch, the triangle formed by the points lies inside the trilateral formed by the lines, as in the left of Figure 1. In terms more amenable to calculation, such a triangle and trilateral are the projectivisations, respectively, of a triple (V_0, V_1, V_2) of vectors in \mathbb{R}^3 and a triple (v_0, v_1, v_2) of covectors such that $v_i \cdot V_j \geq 0$, with equality only when $i = j$.

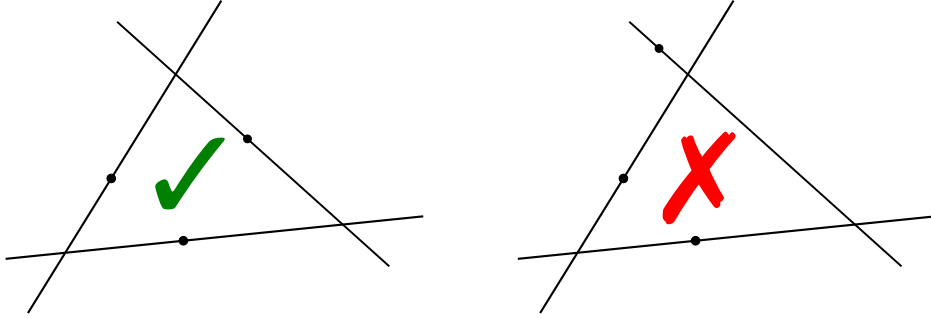


Figure 1: Representatives of an element and a non-element of \mathcal{P}_3^+ .

This is viewed as a pair $(V.\Delta, \Delta.v)$ of left and right cosets of the subgroup Δ of diagonal matrices in $\text{GL}(3, \mathbb{R})$ admitting a representative (V, v) such that $v.V$ is a positive counter-diagonal matrix, i.e. a matrix of the form

$$\begin{pmatrix} 0 & + & + \\ + & 0 & + \\ + & + & 0 \end{pmatrix},$$

where the $+$ entries are positive numbers, possibly different.

Let

$$\sigma = \begin{pmatrix} 0 & 1 & 0 \\ 0 & 0 & 1 \\ 1 & 0 & 0 \end{pmatrix}. \quad (1)$$

If M is positive counter-diagonal, then $\sigma.M.\sigma^{-1}$ is again positive counter-diagonal. The fix-points of this $\mathbb{Z}/3\mathbb{Z}$ action are called *trigonal*. We will show that every element of \mathcal{P}_3^+ admits as representative a pair $(V.\Delta, \Delta.v)$ with $v.V$ being some trigonal matrix. However, the space of trigonal matrices is two-dimensional, and our intent is to show that \mathcal{P}_3^+ is one-dimensional. So we should like to produce, for any such pair, a canonical trigonal matrix. One possible choice of trigonal matrix (with one free parameter) is the *standard trigonal* matrix

$$C_3^f = \begin{pmatrix} 0 & f & 1 \\ 1 & 0 & f \\ f & 1 & 0 \end{pmatrix}. \quad (2)$$

Proposition 2 *Every double coset of the form $\Delta P \Delta$ in $\text{GL}(3, \mathbb{R})$ with P a positive counter-diagonal matrix admits a unique standard trigonal representative.*

Proof Let P be a positive counter-diagonal matrix in $\text{GL}(3, \mathbb{R})$. We need to solve

$$C.P.D = \begin{pmatrix} 0 & f & 1 \\ 1 & 0 & f \\ f & 1 & 0 \end{pmatrix} \quad (3)$$

for C, D , and f . We should end up with a parameter space of solutions for C and D , since we can scale both C and D by scalars, but f should be uniquely determined.

A direct calculation (see §A, Listing 1) shows that (3) admits solutions in C, D, f precisely when

$$f = \left(\frac{P_{01} \cdot P_{12} \cdot P_{20}}{P_{02} \cdot P_{10} \cdot P_{21}} \right)^{1/3},$$

where the P_{ij} are the entries of P . This concludes the proof of the proposition. \blacksquare

Next, assuming that $v.V$ is standard trigonal, we wish to pick $m \in \mathrm{GL}(3, \mathbb{R})$ such that $v.m^{-1}$ and $m.V$ are as nice as possible. To achieve this, we break duality between v and V here and just let $m = V^{-1}$. Even if $v.V$ is not assumed standard trigonal, we have:

Theorem 3 *Suppose $V, v \in \mathrm{GL}(3, \mathbb{R})$ such that $v.V$ is positive counter-diagonal. Let $m = (V.D)^{-1}$, where D is diagonal with $\lambda_0, \lambda_1, \lambda_2$ along its diagonal, and where*

$$\lambda_0^3 = \frac{(v.V)_{12} \cdot (v.V)_{21}}{(v.V)_{10} \cdot (v.V)_{20}}, \quad \lambda_1^3 = \frac{(v.V)_{20} \cdot (v.V)_{02}}{(v.V)_{21} \cdot (v.V)_{01}}, \quad \lambda_2^3 = \frac{(v.V)_{01} \cdot (v.V)_{10}}{(v.V)_{02} \cdot (v.V)_{12}}. \quad (4)$$

Then $m.V.\Delta = \Delta$ and $\Delta.v.m^{-1} = \Delta.C_f^3$, where f is as in the proof of Proposition 2 with $P = v.V$.

Proof By assumption, $v.V$ is positive counter-diagonal. By Proposition 2, there exist C and D such that $C.(v.V).D = (C.v).(V.D)$ are standard trigonal. Then $m = (V.D)^{-1}$ is an element of $\mathrm{GL}(3, \mathbb{R})$ such that the image of (V, v) under m and (I_3, C_f^3) project to the same configuration. This proves the second portion of the theorem, reducing our proof obligations to verifying that D as defined by (4) admits the existence of $C \in \Delta$ such that $(C.v).(V.D)$ is standard trigonal. This can be verified by a direct calculation (see §A, Listings 3 and 4). \blacksquare

5 Developing map and holonomy

Let $S = S_{1,1}$ be a once-punctured torus with a fixed ideal triangulation Δ_* and a fixed orientation. We slightly modify the framework of [12] to parameterise the marked strictly convex projective structures with finite volume on S . We also note that Fock and Goncharov treat the more general space of framed structures with geodesic boundary, of which the finite-volume structures form a proper subset of positive codimension. Lift Δ_* to the universal cover $\phi : \tilde{S} \rightarrow S$, denote the lifted triangulation by $\tilde{\Delta}_*$, and identify the group of deck transformations with $\pi_1(S)$. The developing map $\mathrm{dev} : \tilde{S} \rightarrow \Omega$ for such a structure sends $\tilde{\Delta}_*$ to an ideal triangulation $\tilde{\tau}$ of Ω , which we may assume has straight edges (see [23]). The edges of this ideal triangulation have well-defined endpoints on $\partial\Omega$, and the finite volume condition implies Ω is round, meaning that every point on its boundary admits a unique tangent line (see [8]). Any triangle of $\tilde{\Delta}_*$ therefore inherits an associated combination of three points in $\mathbb{R}P^2$ and three lines through these points such that, by strict convexity of Ω , the triangle formed by these points lies inside the trilateral formed by the lines as in the left of Figure 1.

Associated to the geometric structure is a *holonomy* $\mathrm{hol} : \pi_1(S) \rightarrow \mathrm{SL}(3, \mathbb{R})$ which makes dev equivariant under the action of $\pi_1(S)$. That is, denoting $\Gamma = \mathrm{hol}(\pi_1(S))$, the map dev takes $\pi_1(S)$ -equivalent triangles of $\tilde{\Delta}_*$ to Γ -equivariant triangles of $\tilde{\tau}$ in Ω . Finally, any two such developing maps for the same structure differ by a projectivity. In conclusion, then, for any triangle of Δ_* , we get an associated element of \mathcal{P}_3^+ , and thereby, via Proposition 2 and Theorem 3, a well-defined positive real number f . Likewise, to any oriented edge \tilde{e} of $\tilde{\Delta}_*$, associate the pair (\tilde{t}, \tilde{t}') of triangles in $\tilde{\Delta}_*$, where \tilde{e} is adjacent to both, and where the orientation of \tilde{t} induces the orientation of \tilde{e} . We may suppose that in an affine patch, the images of \tilde{t}, \tilde{t}' , and the flags attached to their vertices, look as shown in Figure 2.

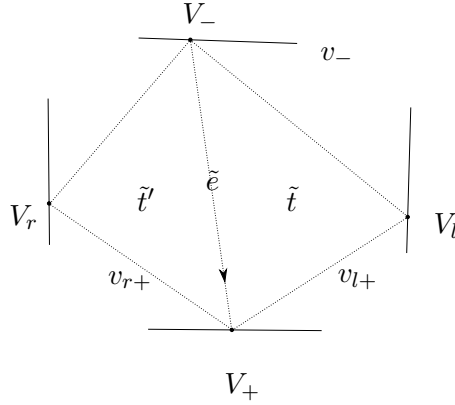


Figure 2: Near the image of an oriented edge \tilde{e} : the labels match the orientation

The flags depicted admit (nonzero) vector-covector representatives (V_i, v_i) for $i \in \{+, -, l, r\}$, such that $v_i \cdot V_i = 0$. Let v_{r+} be a covector representing the line through V_+ and V_r , and likewise let v_{l+} be a covector representing the line through V_+ and V_l . Let v be the matrix whose rows are v_-, v_{r+}, v_{l+} and V the matrix whose columns are V_-, V_r, V_l . Letting $[x], [X]$ denote the projections to $\mathbb{R}P^2$ of covectors x and vectors X , we can associate to this oriented edge \tilde{e} the triple of flags $(([v_-], [V_-]), ([v_{r+}], [V_r]), ([v_{l+}], [V_l]))$, whose projectivity class is some element of \mathcal{P}_3^+ , to which we can associate a single, positive real number f as in the section above. (The *triple ratio* of the triangle defined in [12] equals f^3 . However, our edge parameters' cubes are the *reciprocals* of Fock and Goncharov's edge parameters.)

We may then fix the developing map such that it has the following three properties:

- (1) the standard basis for \mathbb{R}^3 projects to the vertices of $\text{dev}(\tilde{t})$;
- (2) $(1, 0, 0)^t$ and $(0, 1, 0)^t$ project to V_- and V_+ , respectively; and
- (3) the kernels of the covectors $(0, t_{012}, 1)$, $(1, 0, t_{012})$, and $(t_{012}, 1, 0)$ project to lines tangent to the boundary of the convex domain Ω which is the image of the developing map.

This choice of developing map is unique up to isotopy, given our choices of $\phi, \tilde{t}, \tilde{e}$. Hence for each point in $\mathcal{T}_+(S)$ this fixes a unique developing map, and each such developing map determines a unique point in $\mathcal{T}_+(S)$ provided that the holonomy around the cusp is parabolic.

6 Periphery

From the developing map, we may now calculate the holonomy. To this end, it suffices to determine its values on generators of the fundamental group. A marking of $\pi_1(S)$ is chosen as follows. Adjacent to \tilde{t} are three other triangles which project to the same triangle $\phi(\tilde{t}')$ of the ideal triangulation of S . In the cyclic order induced by the orientation of \tilde{t} , let these triangles be c, m, y , with y being the triangle adjacent to \tilde{e} . Then we may choose for generators the deck transformations r, g, b , where r takes m to y , g takes y to c , and b takes c to m .

The images of these deck transformations now are simple to calculate; we just need to calculate representatives (V, v) as above for c, m , and y , and then use Theorem 3 to get the holonomy. We can just focus on y , and the other two will follow by symmetry.

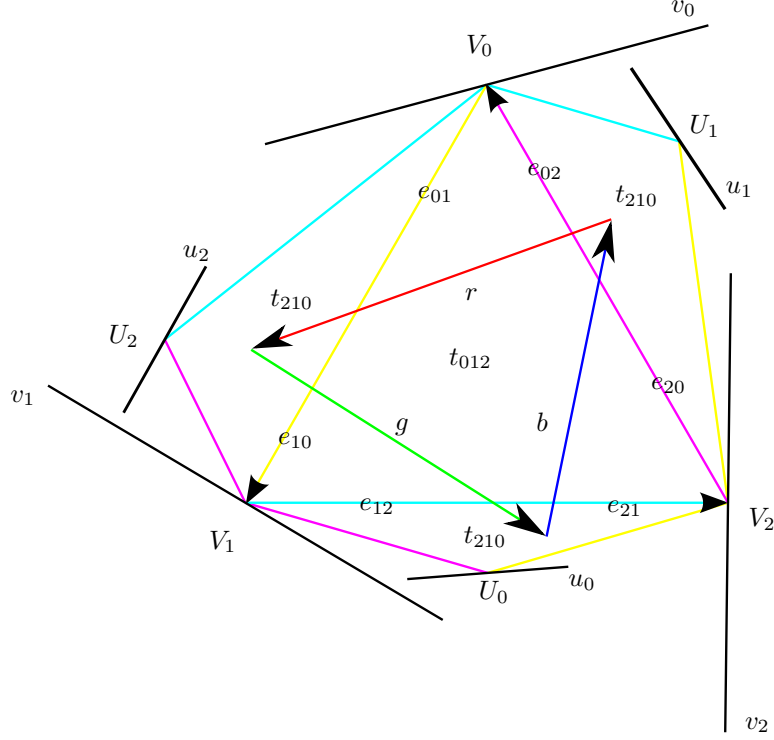


Figure 3: Our standard developing map with labels in our modified framework, where $V_0 = (1 \ 0 \ 0)^t$, $V_1 = (0 \ 1 \ 0)^t$, $V_2 = (0 \ 0 \ 1)^t$, and $v_0 = (0 \ t_{012} \ 1)$, $v_1 = (1 \ 0 \ t_{012})$, $v_2 = (t_{012} \ 1 \ 0)$.

We already know two flags of y : namely, the first two standard basis vectors and the first two associated covectors. To solve for the other vertex of y , we use the edge parameters e_{01} and e_{10} . To solve for the associated line through this vertex, we use the other face parameter and the definition of these parameters as triple ratios. Solving for some element of the vertex of y (regarding the vertex as a one-dimensional subspace of \mathbb{R}^3) gives the vertex U_2 (see §A, Listing 9, for the computation):

$$U_2 = \left\langle \left(\begin{array}{c} (e_{10}^3 + 1) \cdot t_{012}^2 \\ (e_{01}^3 + 1) \cdot e_{10}^3 \\ -e_{10}^3 \cdot t_{012} \end{array} \right) \right\rangle.$$

By symmetry (or by independent calculations), we conclude

$$U_0 = \left\langle \left(\begin{array}{c} -e_{21}^3 \cdot t_{012} \\ (e_{21}^3 + 1) \cdot t_{012}^2 \\ (e_{12}^3 + 1) \cdot e_{21}^3 \end{array} \right) \right\rangle, \quad U_1 = \left\langle \left(\begin{array}{c} (e_{20}^3 + 1) \cdot e_{02}^3 \\ -e_{02}^3 \cdot t_{012} \\ (e_{02}^3 + 1) \cdot t_{012}^2 \end{array} \right) \right\rangle.$$

We have now found the other vertices of our configurations c, m, y , so we have all the triangle parts. Care has to be taken to keep the vertices in a consistent order, so that the holonomy comes out without any extraneous rotation. (Indeed, the holonomy for $S_{0,3}$ differs only in this respect.)

We next need to compute covector representatives of the lines through the U -vertices. We solve for these using the other face parameter t_{210} (see §A, Listings 12 and 13). This gives:

$$u_2 = \langle (e_{01}^3 \cdot e_{10}^3 \quad t_{012}^2 \cdot t_{210}^3 \quad t_{012} \cdot (e_{01}^3 \cdot t_{210}^3 + t_{210}^3 + e_{01}^3 \cdot e_{10}^3 + e_{01}^3)) \rangle$$

and again, by symmetry or independent computation, we conclude

$$u_0 = \langle (t_{012} \cdot (e_{12}^3 \cdot t_{210}^3 + t_{210}^3 + e_{12}^3 \cdot e_{21}^3 + e_{12}^3) \quad e_{12}^3 \cdot e_{21}^3 \quad t_{012}^2 \cdot t_{210}^3) \rangle$$

and

$$u_1 = \langle (t_{012}^2 \cdot t_{210}^3 \quad t_{012} \cdot (e_{20}^3 \cdot t_{210}^3 + t_{210}^3 + e_{20}^3 \cdot e_{02}^3 + e_{20}^3) \quad e_{20}^3 \cdot e_{02}^3) \rangle.$$

Recall that r takes m to y , g takes y to c , and b takes c to m . So with the above results, we can define the trilaterals, completing our construction of the configurations we need for the monodromy calculation (see §A, Listing 14). The formulæ for r , g , and b are complicated and not particularly illuminating, so we leave them in the internals of the computer.

From the above, the fundamental group of $S = S_{1,1}$ has the presentation $\langle r, g, b \mid b \cdot g \cdot r \rangle$ and a fixed marking. The element $r \cdot g \cdot b$ is a peripheral element, representing a simple closed loop around the cusp. As stated in §3, finite volume requires this peripheral element to have parabolic holonomy. This means that its characteristic polynomial is of the form $k \cdot (\lambda - 1)^3$. We may calculate the conditions this imposes on the Fock-Goncharov parameters using the characteristic polynomial. A direct computation (see §A, Listing 15) shows that the characteristic polynomial of $r \cdot g \cdot b$ is proportional to $(\lambda - T^3) \cdot (E^3 \cdot \lambda - T^3) \cdot (T^6 \cdot \lambda - E^3)$, where T is the product of the face parameters and E is the product of the edge parameters. We therefore have:

Lemma 4 *A strictly convex projective structure on $S_{1,1}$ has parabolic peripheral holonomy (and finite volume) if and only if the product of the face parameters and the product of the edge parameters both equal 1.*

To sum up, we now have an identification of $\mathcal{T}_+(S_{1,1})$ with

$$\{(t_{012}, t_{210}, e_{01}, e_{10}, e_{02}, e_{20}, e_{12}, e_{21}) \in \mathbb{R}_+^8 \mid t_{012}t_{210} = 1, e_{01}e_{10}e_{02}e_{20}e_{12}e_{21} = 1\}.$$

7 Cells

An algorithm to compute the ideal cell decompositions of Cooper and Long [3] was recently described by Tillmann and Wong [23], based on an algorithm for hyperbolic surfaces by Weeks [25]. This algorithm takes as starting point a fixed ideal triangulation of $S_{g,n}$ and then computes the canonical ideal cell decomposition associated to a point in moduli space using an edge flipping algorithm followed by possibly deleting redundant edges. This allows one to keep track of the marking, the isotopy class of every intermediate ideal triangulation, and the isotopy class of the final ideal cell decomposition.

We make use of a portion of this work as follows. Let $p = (t_{012}, t_{210}, e_{01}, e_{10}, e_{02}, e_{20}, e_{12}, e_{21}) \in \mathcal{T}_+(S_{1,1})$ and choose a light-cone representative of the cusp; we pick not a standard basis vector, but the slightly different vector

$$S_0 = \begin{pmatrix} e_{20} \cdot e_{02} \cdot e_{21} \\ 0 \\ 0 \end{pmatrix}.$$

This represents the image of the terminal endpoint of \tilde{e} as well as the standard basis vector does. The orbit of this vector under the holonomy of the fundamental group is some collection of vectors, including the elements

$$S_1 = b^{-1} \cdot S_0 = \begin{pmatrix} 0 \\ e_{01} \cdot e_{10} \cdot e_{02} \\ 0 \end{pmatrix}, \quad S_2 = g \cdot S_0 = \begin{pmatrix} 0 \\ 0 \\ e_{12} \cdot e_{21} \cdot e_{10} \end{pmatrix}$$

which represent the other vertices. Note that S_1 represents the initial endpoint of \tilde{e} . Let ω be the covector such that $\omega \cdot S_0 = \omega \cdot S_1 = \omega \cdot S_2 = 1$. Under our assumption of parabolic holonomy, we may write

$$\omega = (e_{01} \cdot e_{10} \cdot e_{12} \quad e_{12} \cdot e_{21} \cdot e_{20} \quad e_{20} \cdot e_{02} \cdot e_{01}).$$

That is, the plane P through S_0, S_1, S_2 is given as $P = \{v : \omega \cdot v = 1\}$.

Then $p \in \mathcal{C}(\Delta_*)$ if and only if for every $\gamma \in \Gamma$ we have $\omega \cdot (\gamma \cdot S_0) \geq 1$, i.e. when every element of the orbit of S_0 does not lie on the same side of P as the origin. It was shown in [23] that it suffices to show this locally, thus turning it into a finite problem. For our purposes, this means that $p \in \mathcal{C}(\Delta_*)$ is equivalent to showing that for all $v \in \{r \cdot S_0, g \cdot S_1, b \cdot S_2\}$, $\omega \cdot v \geq 1$. By construction, $r \cdot S_0 = g^{-1} \cdot S_1$. Therefore call the quantity $\omega \cdot (r \cdot S_0)$ *yellow bending*; we denote yellow bending by YB .¹ We call the condition $YB \geq 1$ *yellow consistency*. In the case of yellow consistency, the convex hull is non-concave along the associated edge. We call the condition $YB = 1$ *yellow flatness*. We make similar definitions for cyan and magenta, with CB and MB being their associated bendings.

Note that if one deletes $\phi(\tilde{e})$ from Δ_* to get an ideal quadrilateral Δ' of S , then for all points p in moduli space, $YB(p) = 1$ is equivalent to $p \in \mathcal{C}(\Delta')$. Likewise for the other edges.

Consistency occurs when all bendings are greater than or equal to one. Now, the bendings are all rational functions, so consistency is a semi-algebraic condition. To show that the set of canonical structures is a cell, we will show the following.

Lemma 5 *The semi-algebraic set determined by the cyan flatness condition is a smooth, properly embedded cell of codimension 1 in $\mathcal{T}_+(S_{1,1})$.*

Lemma 6 *The cyan, yellow and magenta flatness conditions are pairwise disjoint.*

Assuming the lemmata, we can now prove the main theorem:

Proof of Theorem 1 Using our modification of Fock and Goncharov's coordinates as described above, $\mathcal{T}_+(S_{1,1})$ is identified with a properly embedded 6-disc in the positive orthant of \mathbb{R}^8 . Since the action of the mapping class group of $S_{1,1}$ is transitive on the set of all ideal triangulations of $S_{1,1}$, as well as on the set of all ideal quadrilaterals of $S_{1,1}$, it suffices to show that

- (1) one of the sets $\mathring{\mathcal{C}}(\Delta)$, where Δ is an arbitrary but fixed ideal triangulation, is an ideal cell; and
- (2) one of the sets $\mathring{\mathcal{C}}(\Delta')$, where Δ' is an arbitrary but fixed ideal quadrilateral, is an ideal cell.

¹We wish to emphasise that we make the natural choice of using a two letter acronym here.

The latter is the contents of Lemma 5 for Δ' the ideal quadrilateral obtained from Δ_* by deleting the cyan edge. Hence we turn to the former. Let Δ_0 , Δ_1 and Δ_2 denote the three ideal quadrilaterals obtained by deleting one of the three ideal edges from Δ_* . Then the frontier of $\mathring{\mathcal{C}}(\Delta)$ is contained in $\mathring{\mathcal{C}}(\Delta_0) \cup \mathring{\mathcal{C}}(\Delta_1) \cup \mathring{\mathcal{C}}(\Delta_2)$.

For each ideal quadrilateral Δ_i , it follows from Lemma 5 that $\mathring{\mathcal{C}}(\Delta_i)$ is a smooth properly embedded 5-disc. Whence each $\mathring{\mathcal{C}}(\Delta_i)$ cuts $\mathcal{T}_+(S_{1,1})$ into two 6-discs. Now since any two $\mathring{\mathcal{C}}(\Delta_i)$ and $\mathring{\mathcal{C}}(\Delta_j)$ are disjoint by Lemma 6 it follows that $\mathcal{T}_+(S_{1,1}) \setminus \bigcup_i \mathring{\mathcal{C}}(\Delta_i)$ consists of four open 6-discs, and that the one 6-disc with all three 5-discs in its boundary is $\mathring{\mathcal{C}}(\Delta)$.

The statement that $\mathring{\mathcal{C}}$ is a bijection now follows from the well-known fact that any two ideal triangulations of S are related by a finite sequence of edge flips. \blacksquare

Proof of Lemma 5 We can solve $CB = 1$ for e_{20} . (See §A, Listing 19.) Let

$$\top_c = e_{01} \cdot e_{10}^2 \cdot e_{12}^2 \cdot e_{21} \cdot t_{012} - e_{12}^3 - 1, \quad (5)$$

$$\perp_c = e_{21}^3 \cdot t_{012} + t_{012} - e_{01}^2 \cdot e_{10} \cdot e_{12} \cdot e_{21}^2. \quad (6)$$

Then

$$(CB = 1) \equiv (e_{10} \cdot e_{12}^2 \cdot t_{012} \cdot \perp_c \cdot e_{20} = e_{21} \cdot \top_c).$$

So when we project the subset \mathcal{C} cut out by cyan flatness onto the $t_{012}, e_{01}, e_{10}, e_{12}, e_{21}$ plane, the image decomposes into three pieces:

$$(\perp_c > 0 \wedge \top_c > 0) \vee (\perp_c = 0 \wedge \top_c = 0) \vee (\perp_c < 0 \wedge \top_c < 0),$$

with the fiber over every point of the first and last pieces a single point (since we get the graph of $e_{20} = e_{21} \cdot \top_c / (e_{10} \cdot e_{12}^2 \cdot t_{012} \cdot \perp_c)$ over these regions), and the fiber over a point in the middle piece a whole \mathbb{R}_+ .

We will show that the first and last pieces are 5-discs, and that the middle piece is a 3-disc. Then $CB = 1$ will be the union of two 5-discs and a 4-disc (the product of the middle 3-disc with \mathbb{R}_+) in their boundaries; this union is again a 5-disc.

Now, if \sim is one of $<, >, =$, then

$$(\top_c \sim 0) \equiv t_{012} \sim \frac{e_{12}^3 + 1}{e_{01} \cdot e_{10}^2 \cdot e_{12}^2 \cdot e_{21}}, \quad (\perp_c \sim 0) \equiv t_{012} \sim \frac{e_{01}^2 \cdot e_{10} \cdot e_{12} \cdot e_{21}^2}{e_{21}^3 + 1}.$$

Let $p = (e_{12}^3 + 1) / (e_{01} \cdot e_{10}^2 \cdot e_{12}^2 \cdot e_{21})$ and $q = e_{01}^2 \cdot e_{10} \cdot e_{12} \cdot e_{21}^2 / (e_{21}^3 + 1)$. Let \uparrow and \downarrow denote the maximum and minimum operators respectively. The first piece is equivalent to $t_{012} > p \uparrow q$, which is the region above the graph of a function (viz. $p \uparrow q$); this region is a 5-disc.

Now, p and q are both positive functions, assuming their arguments are positive. So the last piece is the region between the graph of a positive function (viz. $p \downarrow q$) and the $e_{01}, e_{10}, e_{12}, e_{21}$ -plane; this is again just a 5-disc.

For the middle piece, one sees that $p = q$ is equivalent to

$$e_{01}^3 = \frac{(e_{12}^3 + 1) \cdot (e_{21}^3 + 1)}{e_{10}^3 \cdot e_{12}^3 \cdot e_{21}^3},$$

which is the graph of a positive function (the cube root of the right-hand side) over \mathbb{R}_+^3 , which is a 3-disc. \blacksquare

Proof of Lemma 6 To show disjointness, it will suffice to show that the projections of $\mathcal{C}(Q_c)$ and $\mathcal{C}(Q_y)$ to the $t_{012}, e_{01}, e_{10}, e_{12}, e_{21}$ -plane are disjoint, where Q_e is the ideal quadrilateral obtained from Δ_* by forgetting e . To that end, we repeat the computation from the proof of the previous lemma for yellow flatness (see §A, Listing 20). Based on this, define

$$\begin{aligned}\top_y &= e_{01} \cdot e_{10}^3 \cdot e_{12}^2 \cdot e_{21} \cdot t_{012} + e_{01} \cdot e_{12}^2 \cdot e_{21} \cdot t_{012} - e_{10}, \\ \perp_y &= e_{01} \cdot t_{012} - e_{01}^3 \cdot e_{10} \cdot e_{12} \cdot e_{21}^2 - e_{10} \cdot e_{12} \cdot e_{21}^2.\end{aligned}$$

The projection of the cyan flat-set to this plane decomposes into the pieces shown earlier, and the projection of the yellow flat-set decomposes likewise.

Algorithms for cylindrical algebraic decomposition can return a list containing a point from every cell of this decomposition. We may run such an algorithm in **Sage** [9] on the intersection of the cyan and yellow flat-set projections (see §A, Listings 21 and 22). The computation used **qepcad**; and the output is a list of a point from every cell in the intersection of the projections to the $t_{012}, e_{01}, e_{10}, e_{12}, e_{21}$ -plane of the cyan and yellow flat-sets. But this list is empty; therefore, their intersection is empty. ■

8 The thrice-punctured sphere

An ideal triangulation of the thrice-punctured sphere also consists of three properly embedded arcs, and hence divides the sphere into two ideal triangles. So there are six edge invariants and two triangle invariants. However, as there are three cusps, there are three holonomy conditions to ensure that the peripheral elements are parabolic. Using the same set-up as in Figure 3, but taking into account that each of the three indicated deck transformations now fixes the respective vertex of the triangle, a direct computation yields an identification of $\mathcal{T}_+(S_{0,3})$ with the set

$$\{(t_{012}, t_{210}, e_{01}, e_{10}, e_{02}, e_{20}, e_{12}, e_{21}) \in \mathbb{R}_+^8 \mid t_{012}t_{210} = 1, e_{01} = \frac{1}{e_{10}} = e_{12} = \frac{1}{e_{21}} = e_{20} = \frac{1}{e_{21}}\},$$

showing that $\mathcal{T}_+(S_{0,3})$ is 2-dimensional as proven by Marquis [19]. We will simply write $(t_{012}, e_{01}) \in \mathcal{T}_+(S_{0,3})$. The result of the convex hull construction of Cooper and Long [3] now depends, for each point in $\mathcal{T}_+(S_{0,3})$, on the lengths of the light-cone representatives for the three cusps, up to scaling all of them by the same factor. Whence there is an ideal cell decomposition of $S_{0,3}$ associated to each point in the *decorated* moduli space $\tilde{\mathcal{T}}_+(S_{0,3})$, and the latter can be identified with the positive orthant in \mathbb{R}^5 .

Using Alexander's trick, it is an elementary exercise to determine that there are exactly four ideal triangulations and three ideal quadrilaterals of $S_{0,3}$. The *flip graph* is the tripod shown in Figure 4, where the quadrilaterals are obtained as intersections of the two pictures at the ends of each dotted arc. Let Δ_* be the ideal triangulation with the property that there is an arc between any two punctures. The punctures are labelled by 0, 1 and 2, and Δ_i is the triangulation obtained from Δ_* by performing an edge flip on the edge not meeting $i \in \{0, 1, 2\}$. Moreover, the mapping class group of $S_{0,3}$ is naturally isomorphic with the group of all permutations of the three cusps.

Theorem 7 *The set*

$$\{\mathring{\mathcal{C}}(\Delta) \mid \Delta \text{ is an ideal cell decomposition of } S_{0,3}\}$$

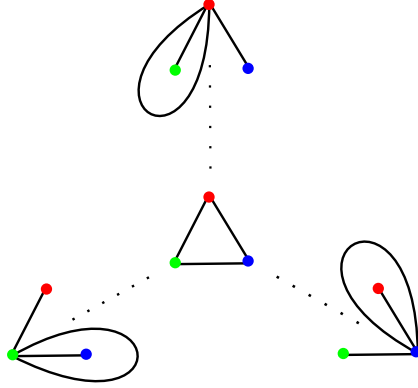


Figure 4: Flip graph of the thrice-punctured sphere

is an ideal cell decomposition of $\tilde{\mathcal{T}}_+(S_{0,3})$ that is invariant under the action of the mapping class group. Moreover, $\mathring{\mathcal{C}}$ is a natural bijection between the cells and the ideal cell decompositions of $S_{0,3}$.

Proof Using the above set-up, let $(e_{01}, t_{012}) \in \mathcal{T}_+(S_{0,3})$, and choose light-cone representatives $V_0 = \begin{pmatrix} \frac{1}{\omega_0} \\ 0 \\ 0 \end{pmatrix}$, $V_1 = \begin{pmatrix} 0 \\ \frac{1}{\omega_1} \\ 0 \end{pmatrix}$, $V_2 = \begin{pmatrix} 0 \\ 0 \\ \frac{1}{\omega_2} \end{pmatrix}$. The corresponding point in $\tilde{\mathcal{T}}_+(S_{0,3})$ is identified with $(t_{012}, e_{01}, \omega_0, \omega_1, \omega_2) \in \mathbb{R}_+^5$.

The three convexity conditions associated to the edges of Δ_* are equivalent to

$$\begin{aligned} \omega_1 - \omega_2 t_{012} + \omega_0 t_{012}^2 &\geq 0, \\ \omega_2 - \omega_0 t_{012} + \omega_1 t_{012}^2 &\geq 0, \\ \omega_0 - \omega_1 t_{012} + \omega_2 t_{012}^2 &\geq 0. \end{aligned}$$

It is interesting to note that these are independent of e_{01} , whence the decomposition is the product of a decomposition of \mathbb{R}^4 with \mathbb{R} . These define $\mathcal{C}(\Delta_*)$. Using these conditions, it is straight forward to check that $\mathcal{C}(\Delta_*)$ is an ideal cell. Moreover,

$$\mathring{\mathcal{C}}(\Delta_0) = \{(t_{012}, e_{01}, \omega_0, \omega_1, \omega_2) \in \mathbb{R}_+^5 \mid \omega_2 - \omega_0 t_{012} + \omega_1 t_{012}^2 < 0\},$$

and likewise for Δ_1 and Δ_2 by cyclically permuting the appropriate subscripts. This divides \mathbb{R}_+^5 into four open 5-balls along three properly embedded open 4-balls, and the dual skeleton to this decomposition is naturally identified with the flip graph of $S_{0,3}$. The invariance by the action of the mapping class group follows since it acts as the group of permutations on $\{0, 1, 2\}$. ■

9 Cloverleaf patches

Of course, we would now like to explore how the geometry of a marked strictly convex projective structure relates to its relative position within a cellular subsets of moduli space, and how the geometry varies as one moves around in moduli space or towards the ‘‘boundary,’’ i.e. as at least one coordinate becomes very small or very large. Structures near the boundary might be difficult to draw properly, given an arbitrary affine patch. The image Ω of the developing map might

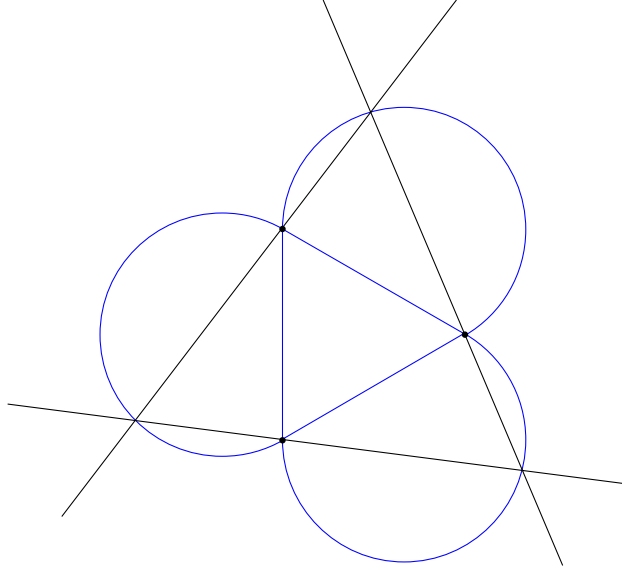


Figure 5: Three vertices and supporting hyperplanes in a cloverleaf patch.

go off to infinity or become thin, yielding uninformative pictures. We must take care, then, with our choice of affine patch. One such choice is *Benzécri position*, discussed in [1, 7]. Our investigations here led us to discover another such choice, which we call a *cloverleaf patch*.

Let S be an oriented marked convex projective surface with geodesic boundary. Let Δ_* be an ideal triangulation of S . Let \tilde{t} and \tilde{e} be an adjacent triangle and edge in the lift $\widetilde{\Delta}_*$ of Δ_* through a universal cover ϕ .

Let dev be the developing map satisfying our choices above, viz.

- (1) the standard basis for \mathbb{R}^3 projects to the image under dev of the vertices of \tilde{t} ;
- (2) $(1, 0, 0)^t$ and $(0, 1, 0)^t$ project to V_- and V_+ , respectively; and
- (3) the kernels of the covectors $(0, t_{012}, 1)$, $(1, 0, t_{012})$, and $(t_{012}, 1, 0)$ project to lines tangent to the boundary of the convex domain Ω that is the image of dev , where t_{012} is the parameter associated to \tilde{t} .

Finally, let

$$\omega = (e_{01} \cdot e_{10} \cdot e_{12} \quad e_{12} \cdot e_{21} \cdot e_{20} \quad e_{20} \cdot e_{02} \cdot e_{01})$$

and let P be the affine patch given by $\omega \cdot v = 1$.

Then P is the *cloverleaf patch* of the structure on S with respect to \tilde{t} and \tilde{e} .

Theorem 8 *Let Ω' be the image of Ω under the affine isomorphism α between a cloverleaf patch and $\mathbb{R}^2 = \mathbb{C}$ that sends the vertices of \tilde{t} to the cube roots of unity and the vertices of \tilde{e} to the primitive cube roots of unity.*

Then Ω' contains the triangle whose vertices are the cube roots of unity, and is contained in the union of unit discs centered at the cube roots of -1 .

Proof The domain Ω' by definition contains the image of \tilde{t} , and the image of \tilde{t} under α is, by definition, the triangle whose vertices are the roots of unity. This concludes the proof of the first claim.

Let

$$\rho = \begin{pmatrix} \frac{e_{20} \cdot e_{02}}{e_{12} \cdot e_{10}} & 0 & 0 \\ 0 & \frac{e_{01} \cdot e_{10}}{e_{20} \cdot e_{21}} & 0 \\ 0 & 0 & \frac{e_{12} \cdot e_{21}}{e_{01} \cdot e_{02}} \end{pmatrix},$$

and let σ be as in (1). Then $\sigma \cdot \rho$ is an element of $\text{SL}(3, \mathbb{R})$ which permutes the vertices of the image of \tilde{t} . But it also permutes the covectors $v_0 = (0 \ t_{012} \ 1)$, $v_1 = (1 \ 0 \ t_{012})$, and $v_2 = (t_{012} \ 1 \ 0)$. We've chosen our developing map so that the kernels of these covectors project to tangent lines to $\partial\Omega$ at the vertices of the image of \tilde{t} . So Ω lies within the trilateral $\tau = \{V : \langle \forall i \in \{0, 1, 2\} : v_i \cdot V > 0\}$. This trilateral is symmetric under $\sigma \cdot \rho$, so its image is symmetric under $s = \alpha \circ \sigma \cdot \rho \circ \alpha^{-1}$. But s is an order 3 affine automorphism of \mathbb{R}^2 permuting the image of the vertices of \tilde{t} , the cube roots of unity. So s is just $2\pi/3$ rotation about the origin. Therefore the image of τ is a trilateral with an order 3 rotational symmetry. Hence it is an equilateral trilateral circumscribed about the equilateral triangle formed by the roots of unity.

Using elementary Euclidean geometry, it is easy to see that this trilateral must lie in the region described, the union of the unit discs centered at cube roots of -1 . (See Figure 5.) Since Ω' lies inside this trilateral, it lies inside the region as well. ■

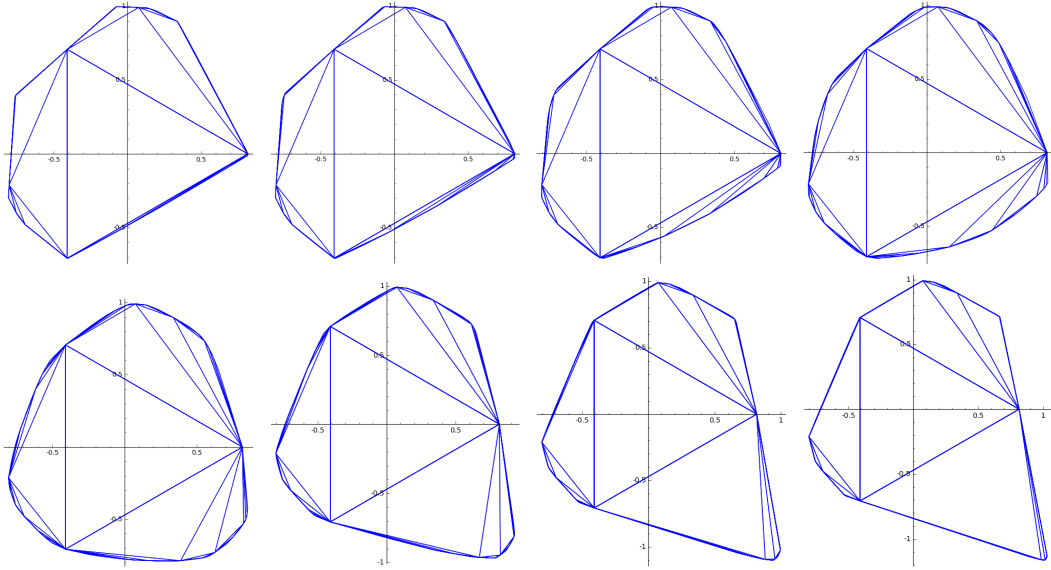


Figure 6: A degenerating sequence of projective structures in cloverleaf position all lying in the same cell of moduli space and with the first and last pictures close to the boundary at infinity. The parameters are $(1/\sqrt[3]{2}, \sqrt[3]{2}, 1, \sqrt[3]{4}, 1, 1, 2^\mu, 2^{-\mu-2/3})$ for $\mu \in \{-2.5 + i/2 : 0 \leq i < 8\}$, and the domains appear to converge to polygons.

This set-up, and the explicit determination of the cell decomposition for $S_{1,1}$, allow a systematic study of deformations and degenerations of strictly convex projective structures on the once-punctured torus, which will be conducted in the future. See Figure 6 for an example.

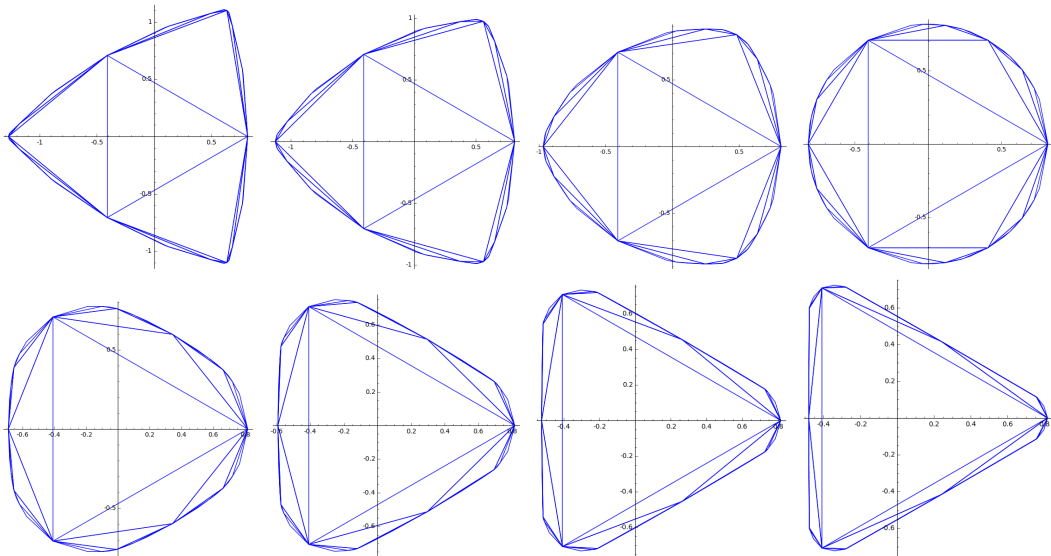


Figure 7: A degenerating sequence of projective structures on $S_{0,3}$ in clover position all lying in the same cell of moduli space and with the first and last pictures close to the boundary at infinity.

Moreover, there is scope to do explicit computations for other surfaces of low complexity—the main issue is that the rational functions appearing in the coordinates of orbits of the vertices of the fundamental domain become more complicated. Such examples are of particular interest because there are different possible approaches to compactifying the moduli space (just as there are different compactifications of Teichmüller space), whose relative merits can be explored with our tools. Moreover, there should be geometric invariants and properties associated with the relative position of a point in moduli space within the cell containing it. Again, it is hoped that our tools can be used to determine, and quantify, such invariants.

10 Conclusion

This paper gives evidence that results known about classical Teichmüller space may have analogues in projective geometry. In this paper, we have focussed on cusped strictly convex projective surfaces and highlighted possible applications in the previous section. More generally, the parameter space due to Fock and Goncharov also parameterises strictly convex projective structures with geodesic boundary. Cell decompositions for the analogous space of hyperbolic structures are known using a variety of approaches; see, for instance, the work of Ushijima [24], Penner [22], Mondello [20], and Guo and Luo [14]. Extending our methods to these more general surfaces would provide a unified framework, in which cusps can open to boundary components, and boundary components shrink to cusps.

An even more tantalising problem arises when going to higher dimensions. The constructions due to Epstein and Penner [10] and Cooper and Long [3] work in arbitrary dimensions. Moreover, there is a canonical cell decomposition of hyperbolic manifolds with boundary due to Kojima [16, 17]. Whereas the moduli space of complete hyperbolic structures on a finite-volume hyperbolic manifold is a single point if the dimension is at least three, the moduli space of strictly

convex projective structures on such a manifold may be larger as shown by Cooper, Long and Thistlethwaite [4, 5, 6]. At the time of writing, it is not clear why some hyperbolic 3-manifolds deform whilst others do not, and the study of the decomposition of the decorated moduli space may hold the key to the answer, as well as shed light on other connections between the geometry and topology of a manifold.

Acknowledgements This research was partially supported by Australian Research Council grant DP140100158.

References

- [1] Jean-Paul Benzécri. Sur les variétés localement affines et localement projectives. *Bull. Soc. Math. France*, 88:229–332, 1960.
- [2] Brian H. Bowditch and David B. A. Epstein. Natural triangulations associated to a surface. *Topology*, 27(1):91–117, 1988.
- [3] Daryl Cooper and Darren D Long. A generalization of the Epstein-Penner construction to projective manifolds. *Proc. Amer. Math. Soc.*, 143(10):4561–4569, 2015.
- [4] Daryl Cooper, Darren D. Long, and Morwen B. Thistlethwaite. Computing varieties of representations of hyperbolic 3-manifolds into $SL(4, \mathbb{R})$. *Experiment. Math.*, 15(3):291–305, 2006.
- [5] Daryl Cooper, Darren D. Long, and Morwen B. Thistlethwaite. Flexing closed hyperbolic manifolds. *Geom. Topol.*, 11:2413–2440, 2007.
- [6] Daryl Cooper, Darren D. Long, and Morwen B. Thistlethwaite. Constructing non-congruence subgroups of flexible hyperbolic 3-manifold groups. *Proc. Amer. Math. Soc.*, 137(11):3943–3949, 2009.
- [7] Daryl Cooper, Darren D. Long, and Stephan Tillmann. Deforming convex projective manifolds. *arXiv e-prints*, arXiv:1511.06206, 2015.
- [8] Daryl Cooper, Darren D. Long, and Stephan Tillmann. On convex projective manifolds and cusps. *Adv. Math.*, 277:181–251, 2015.
- [9] The Sage Developers. *Sage Mathematics Software (Version 6.9)*, 2015. <http://www.sagemath.org>.
- [10] David B. A. Epstein and Robert C. Penner. Euclidean decompositions of noncompact hyperbolic manifolds. *J. Differential Geom.*, 27(1):67–80, 1988.
- [11] William J. Floyd and Allen Hatcher. Incompressible surfaces in punctured-torus bundles. *Topology Appl.*, 13(3):263–282, 1982.
- [12] Vladimir V. Fock and Alexander B. Goncharov. Moduli spaces of local systems and higher Teichmüller theory. *Publ. Math. Inst. Hautes Études Sci.*, 103:1–211, 2006.
- [13] Vladimir V. Fock and Alexander B. Goncharov. Moduli spaces of convex projective structures on surfaces. *Adv. Math.*, 208(1):249–273, 2007.
- [14] Ren Guo and Feng Luo. Cell decompositions of Teichmüller spaces of surfaces with boundary. *Pacific J. Math.*, 253(2):423–438, 2011.
- [15] John L. Harer. The virtual cohomological dimension of the mapping class group of an orientable surface. *Invent. Math.*, 84(1):157–176, 1986.
- [16] Sadayoshi Kojima. Polyhedral decomposition of hyperbolic manifolds with boundary. In *On the Geometric Structure of Manifolds*, edited by Dong Pyo Chi, volume 10, part III, of *Proceedings of Workshops in Pure Mathematics*, pages 37–57. Seoul National University, Korea, 1990.

- [17] Sadayoshi Kojima. Polyhedral decomposition of hyperbolic 3-manifolds with totally geodesic boundary. In *Aspects of low-dimensional manifolds*, volume 20 of *Adv. Stud. Pure Math.*, pages 93–112. Kinokuniya, Tokyo, 1992.
- [18] Marc Lackenby. The canonical decomposition of once-punctured torus bundles. *Comment. Math. Helv.*, 78:363–384, 2003.
- [19] Ludovic Marquis. Espace des modules marqués des surfaces projectives convexes de volume fini. *Geom. Topol.*, 14(4):2103–2149, 2010.
- [20] Gabriele Mondello. Triangulated Riemann surfaces with boundary and the Weil-Petersson Poisson structure. *J. Differential Geom.*, 81(2):391–436, 2009.
- [21] Robert C. Penner. The decorated Teichmüller space of punctured surfaces. *Comm. Math. Phys.*, 113(2):299–339, 1987.
- [22] Robert C. Penner. Decorated Teichmüller theory of bordered surfaces. *Comm. Anal. Geom.*, 12(4):793–820, 2004.
- [23] Stephan Tillmann and Sampson Wong. An algorithm for the Euclidean cell decomposition of a cusped strictly convex projective surface. *Journal of Computational Geometry*, 7:237–255, 2016.
- [24] Akira Ushijima. A canonical cellular decomposition of the Teichmüller space of compact surfaces with boundary. *Comm. Math. Phys.*, 201(2):305–326, 1999.
- [25] Jeffrey R. Weeks. Convex hulls and isometries of cusped hyperbolic 3-manifolds. *Topology Appl.*, 52(2):127–149, 1993.

School of Mathematics and Statistics F07
The University of Sydney
NSW 2006 Australia
robert.haraway@sydney.edu.au
stephan.tillmann@sydney.edu.au

A Code Listings

Listing 1: Maxima code, part 0

```

matrixEq(M,N) :=
  block ([mr:length(M),mc:length(M[1]),
         nr:length(N),nc:length(N[1]),
         eqs:[],i,j],
         if mr = nr and mc = nc
         then for i:1 thru mr step 1 do
              for j:1 thru mc step 1 do
                  eqs:cons(M[i][j]=N[i][j],eqs)
         else [],
         eqs)$
P : matrix([0,P01,P02],
           [P10,0,P12],
           [P20,P21,0])$
C : matrix([C0,0,0],[0,C1,0],[0,0,C2])$
D : matrix([D0,0,0],[0,D1,0],[0,0,D2])$
goal : matrix([0,f,1],[1,0,f],[f,1,0])$
pcdsols : solve(matrixEq(C.P.D,goal),[f,C0,C1,C2,D0,D1,D2])[3]$
print(pcdsols[1]);

```

(N.B. Maxima does not solve matrix equations, necessitating the little for loop routine.)

Listing 2: Maxima code, output 0

$$f = \frac{\begin{matrix} 1/3 & 1/3 & 1/3 \\ P01 & P12 & P20 \end{matrix}}{\begin{matrix} 1/3 & 1/3 & 1/3 \\ P02 & P10 & P21 \end{matrix}}$$

Listing 3: Maxima code, part 1

```

symmsols : subst(P21^(1/3)*P12^(1/3)*P20^(-1/3)*P10^(-1/3),%r3,
                pcdsols)$
symmsols[5];symmsols[6];symmsols[7];

```

Listing 4: Maxima code, output 1

$$D0 = \frac{\begin{matrix} 1/3 & 1/3 \\ P12 & P21 \end{matrix}}{\begin{matrix} 1/3 & 1/3 \\ P10 & P20 \end{matrix}}$$
$$D1 = \frac{\begin{matrix} 1/3 & 1/3 \\ P02 & P20 \end{matrix}}{\begin{matrix} 1/3 & 1/3 \\ P01 & P21 \end{matrix}}$$
$$D2 = \frac{\begin{matrix} 1/3 & 1/3 \\ P01 & P10 \end{matrix}}{\begin{matrix} 1/3 & 1/3 \\ P02 & P12 \end{matrix}}$$

Listing 5: Maxima code, part 2

```
mapToStdTrigon(V,v) :=
  block ([vV, L0, L1, L2, D, m],
    vV : v.V,
    L0 : (vV[2][3] * vV[3][2])^(1/3)/(vV[2][1] * vV[3][1])^(1/3),
    L1 : (vV[3][1] * vV[1][3])^(1/3)/(vV[3][2] * vV[1][2])^(1/3),
    L2 : (vV[1][2] * vV[2][1])^(1/3)/(vV[1][3] * vV[2][3])^(1/3),
    D : matrix([L0,0,0],
               [0,L1,0],
               [0,0,L2]),
    m : invert(V.D),
    determinant(m)^(-1/3)*m)$
projFromTo(V,v,W,w) := invert(mapToStdTrigon(W,w)) .
                           mapToStdTrigon(V,v)$
```

We already know two flags of y : namely, the first two standard basis vectors and the first two associated covectors. This is the content of listing 6.

Listing 6: Maxima code, part 3

```
V0 : matrix([1],[0],[0])$
v0 : matrix([0,t012,1])$
V1 : matrix([0],[1],[0])$
v1 : matrix([1,0,t012])$
V2 : matrix([0],[0],[1])$
v2 : matrix([t012,1,0])$
```

The equations we solve are just our definitions of the parameters as triple ratios, so we had better code in triple ratios as well. Listing 7 takes this into consideration.

Listing 7: Maxima code, part 4

```
R3(v,V) :=
  block([vV:v.V],
    vV[1][2]*vV[2][3]*vV[3][1]/
    (vV[1][3]*vV[2][1]*vV[3][2]))$
trilateral(p,q,r) := addrow(addrow(p,q),r)$
triangle(P,Q,R) := addcol(addcol(P,Q),R)$

tr(P,p,Q,q,R,r) := R3(trilateral(p,q,r),triangle(P,Q,R))$
```

Listing 8: Maxima code, part 5

```
maprhs(listofeqs) := create_list(rhs(eq),eq,listofeqs)$
```

In a functional programming language like Haskell we could write (`map rhs`) and skip listing 8.

Listing 9: Maxima code, part 6

```
U2repEqs : block([UU,UUV0,UUV1,V2V0,V2V1,e01eq,e10eq,fullsol,Usol],
  UU : matrix([UU0],[UU1],[UU2]),
  UUV0 : matrix([UUV00,UUV01,UUV02]),
  UUV1 : matrix([UUV10,UUV11,UUV12]),
  V2V0 : matrix([0,1,0]),
  V2V1 : matrix([1,0,0]),
  e01eq : e01^3 = tr(V0,v0,UU,UUV1,V2,V2V1),
  e10eq : e10^3 = tr(V1,v1,V2,V2V0,UU,UUV0),
  subst((e10^3+1)*t012^2,%r8, solve([e01eq,e10eq,UUV0.UU=0,UUV0.V0=0,
    UUV1.UU=0,UUV1.V1=0],
    [UU0,UU1,UU2,
    UUV00,UUV01,UUV02,
    UUV10,UUV11,UUV12])[2]));
```

N.B. we are allowed to substitute what we like for `%r8` because of our scalar freedom in choosing a representative of U_2 , and we choose Maxima's second solution since the other solutions are spurious.

The next listing incorporates the values of U_0 , U_1 and U_2 .

Listing 10: Maxima code, part 7

```
U2rep : matrix([(e10^3 + 1)*t012^2],
  [(e01^3 + 1)*e10^3],
  [-e10^3*t012]);
sigma3 : matrix([0,0,1],
  [1,0,0],
  [0,1,0]);
U0rep : sigma3.sublis([e10=e21,e01=e12],U2rep);
U1rep : sigma3.sublis([e21=e02,e12=e20],U0rep);
```

We have now found the other vertices of our configurations c, m, y , so we have all the triangle parts. Listing 11 expresses this.

Listing 11: Maxima code, part 8

```
Y : triangle(U2rep, V1, V0)$
C : triangle(V1, U0rep, V2)$
M : triangle(V0, V2, U1rep)$
```

Listing 12: Maxima code, part 9

```
uu : matrix([uu0, uu1, uu2])$
yy : trilateral(uu, v1, v0)$
factor(subst(t012^2*t210^3,%r35,
            solve([R3(yy, Y)=t210^3, uu.U2rep=0],
                  [uu0, uu1, uu2]))[1]);
```

The next listing incorporates the computation of the covectors.

Listing 13: Maxima code, part 10

```
u2rep : matrix([e01^3*e10^3, t012^2*t210^3,
               t012*(e01^3*t210^3 + t210^3 + e01^3*e10^3 + e01^3)]);
u0rep : sublis([e01=e12, e10=e21], u2rep).invert(sigma3);
ulrep : sublis([e12=e20, e21=e02], u0rep).invert(sigma3);
```

Listing 14: Maxima code, part 11

```
y : trilateral(u2rep, v1, v0)$
c : trilateral(v1, u0rep, v2)$
m : trilateral(v0, v2, ulrep)$

r : factor(projFromTo(M, m, Y, y))$
g : factor(projFromTo(Y, y, C, c))$
b : factor(projFromTo(C, c, M, m))$
```

Listing 15: Maxima code, part 12

```
perph : r.g.b$
factor(charpoly(perph, lambda));
```

Listing 16 phrases the contents of Lemma 4 in code, assuming all variables are positive.

Listing 16: Maxima code, part 13

```
parhol : [t210 = 1/t012, e02 = 1/(e01*e10*e12*e21*e20)]$
```

The next listing summarises the choice of light-cone representatives in §7.

Listing 17: Maxima code, part 14

```
S0 : matrix([e20*e02*e21], [0], [0])$
S1 : matrix([0], [e01*e10*e02], [0])$
S2 : matrix([0], [0], [e12*e21*e10])$
omega : matrix([e01*e10*e12, e12*e21*e20, e20*e02*e01])$
```

The next listing encodes the bendings, using the semantics of subtractive primary colours.

Listing 18: Maxima code, part 15

```
YB : omega.r.S0$
YB : factor(YB);
CB : omega.g.S1$
CB : factor(CB);
MB : omega.b.S2$
MB : factor(MB);
```

Listing 19: Maxima code, part 16

```
factor(solve(sublis(parhol,CB)=1,[e20]));
```

Listing 20: Maxima code, part 17

```
factor(solve(sublis(parhol,YB)=1,[e20]));
```

Algorithms for cylindrical algebraic decomposition can return a list containing a point from every cell of this decomposition. We run such an algorithm in Sage [9] on the intersection of the cyan and yellow flat-set projections as in listing 21, returning as output listing 22. The first line is just from the declaration of variables. The last line is the output of `qepcad`; it is a list of a point from every cell in the intersection of the projections to the $t_{012}, e_{01}, e_{10}, e_{12}, e_{21}$ -plane of the cyan and yellow flat-sets. But this list is empty; therefore, their intersection is empty.

Listing 21: SAGE code

```
# SAGE code for disjointness
qf = qepcad_formula
var('t012,e01,e10,e12,e21')

top_c = e01*e10^2*e12^2*e21*t012 - e12^3 - 1
bot_c = e21^3*t012 + t012 - e01^2*e10*e12*e21^2
cyan_pos = qf.and_(top_c > 0, bot_c > 0)
cyan_neg = qf.and_(top_c < 0, bot_c < 0)
cyan_0 = qf.and_(top_c == 0, bot_c == 0)

top_y = e01*e10^3*e12^2*e21*t012 + e01*e12^2*e21*t012 - e10
bot_y = e01*t012 - e01^3*e10*e12*e21^2 - e10*e12*e21^2
yell_pos = qf.and_(top_y > 0, bot_y > 0)
yell_neg = qf.and_(top_y < 0, bot_y < 0)
yell_0 = qf.and_(top_y == 0, bot_y == 0)

all_pos = qf.and_(t012>0, e01>0, e10>0, e12>0, e21>0)

cyan = qf.and_(all_pos, qf.or_(cyan_pos, cyan_0, cyan_neg))
yellow = qf.and_(all_pos, qf.or_(yell_pos, yell_0, yell_neg))

qepcad(qf.and_(cyan, yellow), solution='cell-points')
```

Listing 22: SAGE output

```
(t012, e01, e10, e12, e21)
[]
```